Journal of Neuroscience Methods 295 (2018) 10–19

Contents lists available at ScienceDirect

Journal of Neuroscience Methods

journal homepage: www.elsevier.com/locate/jneumeth

# Arterial spin labeling perfusion MRI signal denoising using robust principal component analysis

Hancan Zhu [a], Jian Zhang [b], Ze Wang [b,c,*]

[a] School of Mathematics Physics and Information, Shaoxing University, Shaoxing, 312000, China
[b] Center for Cognition and Brain Disorders, Institutes of Psychological Science, Hangzhou Normal University, Hangzhou, 310010, China
[c] Department of Radiology, Lewis Katz School of Medicine, Temple University, Philadelphia, PA 19140, USA

## HIGHLIGHTS

- We proposed a new arterial spin labeling perfusion MRI signal denoising method using robust principal component analysis.
- The proposed method markedly increased temporal signal-to-noise-ratio (TSNR).
- The proposed method increased the sensitivity of ASL CBF images for FC analysis and task activation detection.

## ARTICLE INFO

*Article history:*
Received 11 August 2017
Received in revised form
24 November 2017
Accepted 27 November 2017
Available online 28 November 2017

*Keywords:*
Arterial spin labeling
Temporal denoising
Robust principal component analysis
Functional connectivity

## ABSTRACT

*Background:* Arterial spin labeling (ASL) perfusion MRI provides a non-invasive way to quantify regional cerebral blood flow (CBF) and has been increasingly used to characterize brain state changes due to disease or functional alterations. Its use in dynamic brain activity study, however, is still hampered by the relatively low signal-to-noise-ratio (SNR) of ASL data.
*New method:* The aim of this study was to validate a new temporal denoising strategy for ASL MRI. Robust principal component analysis (rPCA) was used to decompose the ASL CBF image series into a low-rank component and a sparse component. The former captures the slowly fluctuating perfusion patterns while the latter represents spatially incoherent spiky variations and was discarded as noise. While there still lacks a way to determine the parameter for controlling the balance between the low-rankness and sparsity of the decomposition, we designed a method to solve this problem based on the unique data structures of ASL MRI. Method evaluations were performed with ASL CBF-based functional connectivity (FC) analysis and a sensorimotor functional ASL MRI study.
*Comparison with existing method(s):* The proposed method was compared with the component based noise correction method (CompCor).
*Results:* The proposed method markedly increased temporal signal-to-noise-ratio (TSNR) and sensitivity of ASL CBF images for FC analysis and task activation detection.
*Conclusions:* We proposed a new temporal ASL CBF image denoising method, and showed its benefit for the CBF time series-based FC analysis and task activation detection.


## 1. Introduction

Arterial spin labeling (ASL) perfusion MRI provides a non-invasive approach to quantify cerebral blood flow (CBF) (Detre et al., 1992). Using the magnetically labeled arterial blood as the endogenous tracer, ASL MRI produces the perfusion-weighted signal by subtracting brain images acquired after the tracer enters the imaging location from those acquired without tracer modulations (in the control condition), which is subsequently converted into the quantitative CBF in a unit of ml/100 mg/min using an appropriate compartment model (Alsop et al., 2015). Spin labeling and control labeling are generally repeated multiple times to calculate the mean CBF map or to produce the CBF image series for time series analysis such as functional task activation study or functional connectivity (FC) analysis. Due to the technique advances made over the past decades, ASL MRI is now available in all mainframe MR vendors. The two most widely used ASL techniques are the pulsed

* Corresponding author at: Center for Cognition and Brain Disorders, Hangzhou Normal University, Wenzhou Road 126, Building 7, 2nd floor, Hangzhou, Zhejiang Province, China/3401N Broad St, 1st Floor, Radiology, Philadelphia, PA 19140, USA.
*E-mail addresses:* zewangnew@163.com, zewangnew@temple.edu (Z. Wang).

https://doi.org/10.1016/j.jneumeth.2017.11.017
0165-0270/

ASL (PASL) (Kim, 1995; Siewert et al., 1997; Wong et al., 1997) and pseudo continuous ASL (PCASL) (Dai et al., 2008). PASL tags the arterial spins using a very short inversion RF pulse, and PCASL is a modern extension to the traditional continuous ASL (Detre et al., 1992), which tags the arterial spins using many successive small RF pulses in a plane proximal to the tissue to be imaged (Dai et al., 2008). Because the labeling duration is longer in PCASL (and CASL) than in PASL, PCASL perfusion MRI presents higher signal-to-noise ratio (SNR) (Alsop et al., 2015). After spin labeling, ASL signal can be acquired with any MRI sequence. A widely used imaging sequence in ASL is the two-dimensional (2D) echo-planar imaging (EPI), but 3D acquisition sequences are now more preferred because of the capability of adding additional RF pulses to optimally suppress background signal for the entire brain in order to maximally improve the SNR of ASL data (Fernández-Seara et al., 2005; Maleki et al., 2012; Vidorreta et al., 2017, 2012; Ye et al., 2000) though the single-shot acquisition still suffers from T2-decay blurring along the partition acquisition direction(Chang et al., 2017; Vidorreta et al., 2017).

Limited by the longitudinal relaxation rate (T1) of arterial blood water and the post-labeling transmit time, only a small fraction of tissue water can be replaced with the labeled arterial spins. As a result, the perfusion signal acquired in ASL MRI (the difference between the labeled and control images) is only about a few percent of the background signal, resulting in a very low SNR (Wong, 1999). This situation is even severer in the case of ASL CBF time series-based functional studies since the activation-induced ASL perfusion signal changes generally only accounts for a few tenths of the small fraction of baseline signal change. In the past, various ASL data denoising methods have been proposed (Behzadi et al., 2007; Bibic et al., 2010; Chuang et al., 2008a; Liang et al., 2015; Liu and Wong, 2005; Maumet et al., 2014; Wang, 2012, 2014; Wang et al., 2005, 2008, 2007, 2013; Wells et al., 2010) for either reducing spatial noise, removing outlier time points, or suppressing temporal nuisances, but no one has explicitly considered both the spatial and temporal noise simultaneously.

As a physiological measure, CBF shows high correlation between neighboring voxels especially when they belong to the same functional brain region. A reasonable extension to this spatial coherence assumption is that the whole brain CBF map should be highly correlated across time. In other words, the CBF image series should present slow fluctuations across space and time. Those sparsely distributed variations with large magnitude are more likely contributed by noise. This low-rank (slowly varying) signal + sparse noise data structure may not be optimally processed using previously published temporal ASL denoising methods (Behzadi et al., 2007; Restom et al., 2006; Wang, 2012; Wu et al., 2009). Robust principal component analysis (rPCA) (Candès et al., 2011) is an emerging multivariate signal decomposition algorithm, which has been increasingly used in many kinds of image processing (Candès et al., 2011), image denoising (Fang et al., 2015), and fast MRI imaging (Chiew et al., 2015; Otazo et al., 2015; Singh et al., 2015). Sorting all acquired data into a big data matrix, rPCA decomposes the original data into a low-rank (L) plus a sparse (S) component with the same data dimensions. The L-component represents the slowly varying part and the S-component carries the temporally uncorrelated dynamic changes. Such process fits well with the above mentioned spatio-temporal feature of ASL CBF images (Aguirre et al., 2002).

The purpose of this paper was to assess rPCA (or equivalently the L + S decomposition) as a potential spatio-temporal ASL denoising method (LS-ASLd). We first performed numerical experiment to identify an optimal parameter for L + S decomposition. We then compared LS-ASLd to currently available ASL denoising methods in terms of TSNR. We expected to see that increased TSNR by LS-ASLd would contribute higher sensitivity in the functional connectivity (FC) analysis, which has been a hot topic for a while. A pilot development of this method was recently presented in a conference abstract (Wang, 2016).

## 2. Methods

### 2.1. Subjects

Representative ASL data were identified from existing database in our laboratory, containing the resting state ASL data and the task ASL data. For the resting state ASL data, thirty young healthy subjects (age: 22–28, 12 males) were included, in which ten subjects were used for selecting best parameters and the rest twenty subjects were used for validating the efficacy of the proposed method. For the task ASL data, thirteen subjects (age: 23–30, 7 males) were included. Data acquisition and re-use were approved by local Internal Review Board (IRB). Subjects provided IRB approved signed consent forms before data acquisition.

### 2.2. Image acquisition

MR imaging was conducted in a 3-T whole-body scanner (Siemens Medical Systems, Erlangen, Germany). High-resolution structural images were acquired for spatial brain normalization using a 3D MPRAGE sequence (TR/TE/TI = 1620/3/950 ms, voxel size = 1 $mm^3$). Resting ASL perfusion MRI was acquired using a 2D gradient-echo planar imaging-based pseudo-continuous ASL (PCASL) sequence (Dai et al., 2008). 40 control/label image pairs were acquired with parameters of: labeling time = 1.48 s, post-labeling delay = 1.5 s, in plane field-of-view (FOV) = 22 × 22 $cm^2$, matrix = 64 × 64, bandwidth = 3004 Hz/pixel, flip angle = 90°, TR/TE = 4000/11 ms, 20 slices with a thickness of 5 mm plus 1 mm gap. The task ASL MRI was performed before we implemented the PCASL sequence and data acquisition was done with an amplitude modulated continuous ASL sequence with parameters of: labeling time = 1600 ms, post-labeling delay = 800 ms, FOV = 22 × 22 $cm^2$, matrix = 64 × 64, bandwidth = 2046 Hz/pixel, flip angle = 90°, TR = 3000 ms, TE = 17 ms, 12 slices with a slice thickness of 7 mm and an inter-slice gap of 1.25 mm. The scan duration was 7.2 min. Subjects were asked to perform a self-paced right hand finger-tapping task when they saw the visual stimuli on the screen. The stimuli consisted of 3 task blocks interleaved with a grey screen no-task baseline block. Each block lasted for 1.2 min and the visual stimuli during the task blocks were a series of reversing black and white checkerboard flashing in a frequency of 8 Hz.

### 2.3. Data preprocessing

Data preprocessing was performed using the SPM12 (http://www.fil.ion.ucl.ac.uk/spm) based batch scripts provided in ASLtbx (Wang et al., 2008). The following steps were included in both currently existing methods and the proposed LS-ASLd method: the origins of both structural and raw ASL images were first set to be the center of the image matrix; ASL images were then realigned to correct head motions using the customized ASL MRI motion correction method (Wang et al., 2008); ASL images were registered to the structural image for each subject; ASL images were smoothed with an isotropic Gaussian filter with a full-width-at-half-maximum (FWHM) = 6 $mm^3$.

For currently existing methods, temporal noise filtering was performed using high-pass filtering with a cutoff of 0.01 Hz and then the component based noise correction method (CompCor) (Behzadi et al., 2007) and the global signal regression method (Wang, 2012). Without ambiguity, CompCor means all these temporal denoising steps in the rest of the text. Then, each denoised control image was subtracted by its corresponding denoised label

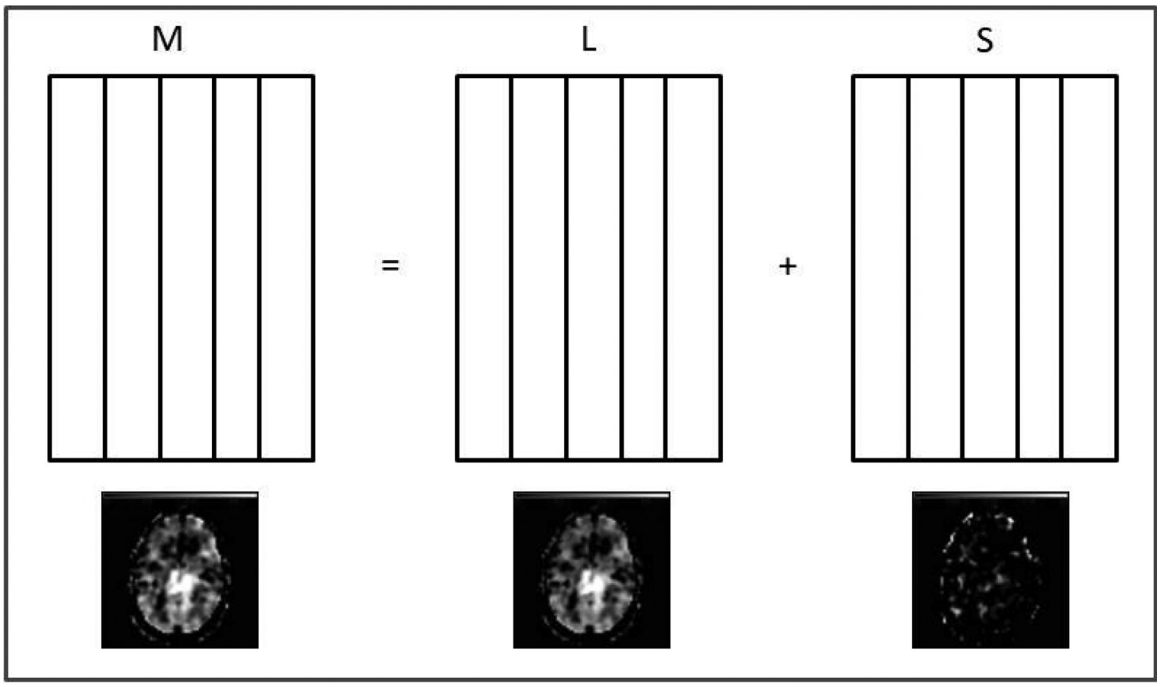


**Fig. 1.** Illustration of the L+S decomposition on ASL CBF images. Each column vector in the matrix M, L, and S represents a reformatted CBF map (by stacking all pixels of the 3-dimensional image into a long column vector sequentially from x, y, and z direction), its low-rank component, and its sparse component, at each timepoint with the same temporal order. In each matrix, the row dimension corresponds to the spatial dimension of ASL CBF images, and the column dimension corresponds to the temporal dimension of ASL CBF images. The 3 image slices beneath the matrices are one representative slice of one CBF map, its L, and S component after reformatting the column vectors back to the 3-dimensional images, respectively.

image to get ASL CBF maps. For the proposed LS-ASLd method, without any temporal denoising, each control image was subtracted by its corresponding label image to get ASL CBF maps. Then, LS-ASLd method was applied to the ASL CBF maps.

### 2.4. rPCA-based ASL CBF image denoising

Fig. 1 illustrates the LS-ASLd process. ASL CBF map (3D) at each timepoint was reformatted into a column vector in the composite data matrix M, which was subsequently decomposed into a low-rank part L and a sparse part S using the L + S decomposition model (Candès et al., 2011):

$$\min_{L,S}\|L\|_* + \lambda\|S\|_1, \text{ subject to } M = L + S, \quad (1)$$

where $\|\cdot\|_*$ denotes the nuclear norm of a matrix, $\|\cdot\|_1$ denotes the sum of the absolute values of matrix entries, and $\lambda$ is a positive weighting parameter. The above optimization problem is well posed and has a unique solution if it satisfies the incoherence condition between L and S, that is, the low-rank matrix L is not sparse and the sparse matrix S is not low-rank (Candès et al., 2011). Various algorithms exist for L + S decomposition. In this paper, we used the inexact augmented Lagrange multiplier rPCA algorithm (Lin et al., 2010). After solving the optimization problem (1), column vectors of the low-rank part L and the sparse part S were reformatted back to the 3-dimensional images, in which the low-rank part was reserved as the denoised CBF images and the sparse part was treated as noise.

### 2.5. Parameter selection

The weighting parameter $\lambda$ in model (1) controls the balance between the low-rankness and sparsity. A small $\lambda$ will add a strong restriction on the low-rank term $\|L\|_*$. As a result, part of CBF signal will be shifted from the low-rank component to the sparse component and discarded as noise. By contrast, a big $\lambda$ will pose a strong restriction on the sparse term $\|S\|_1$, and most of noise will be retained in the low-rank part. In (Candès et al., 2011), the parameter $\lambda$ is set to $\lambda = m^{-1/2}$, where $m$ is the row dimension of the data matrix M. That empirical setting can be changed into $\lambda = \alpha m^{-1/2}$ by adding a scalar multiplier $\alpha$, which enables an easy analysis of the effects of $\lambda$ on the subsequent L+S decomposition. Fig. 2 shows that the sparse component contains more CBF signal when $\alpha$ decreases and becomes sparser when $\alpha$ increases. It is then a practical question for which value of $\alpha$ then $\lambda$ should the decomposition use.

While there is no gold standard for defining the optimal value of $\lambda$, an empirical strategy was designated by incorporating prior information about the ASL CBF data. In the gradient-echo weighted *epi*-based ASL, the acquired control and label images still contain the blood-oxygen-level-dependent (BOLD) fMRI signal, which can be treated as pseudo BOLD data (Aguirre et al., 2002). In BOLD fMRI, a well-established literature is the seed-based functional connectivity (FC) analysis (Biswal and Ulmer, 1999), which has been shown to yield very stable FC patterns(Li et al., 2012; Liao et al., 2013; Meindl et al., 2010). Since the label and control ASL images were acquired one TR apart, they should be able to identify similar FC patterns after correcting the timing difference using interpolation. With temporal denoising, the overlap ratio between their FC patterns should become bigger and stay at a certain level without much significant variations after a turning point. That turning point can be taken as a surrogate "optimal" point for determining the optimal value of $\lambda$. In this paper, L + S decompositions with the same range of $\lambda$ values (with $\alpha$ = 0.25, 0.5, 0.625, 0.75, 0.875, 1, 1.25, 1.5, 1.75, 2, 4, 8) were performed for the control image series and label image series separately. After spatially registering the low rank image series into the Montreal Neurological Institute (MNI) standard brain space, a seed-based FC analysis was conducted using the seed defined in motor-cortex. The mean time series within the seed was extracted as the regressor which was correlated with the

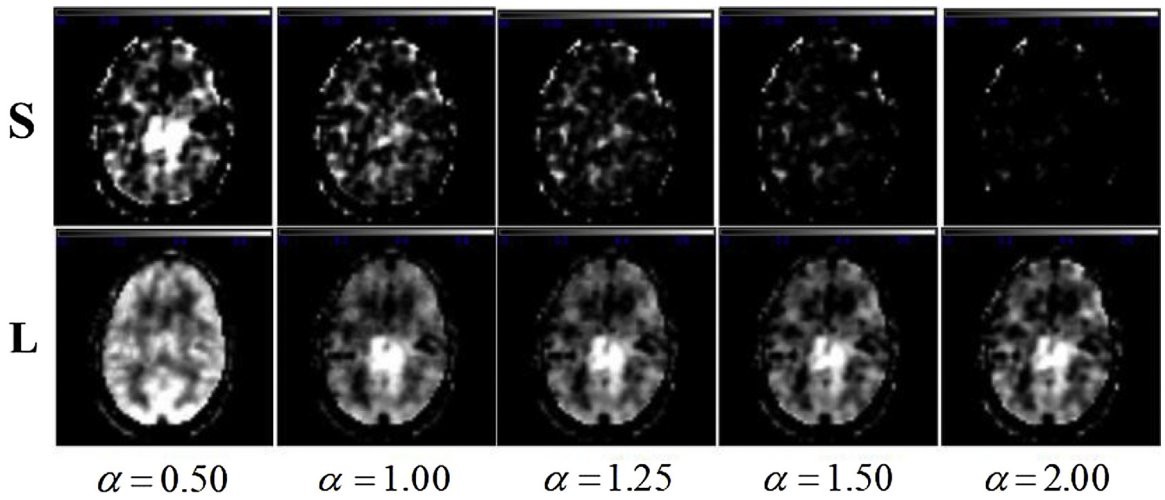


**Fig. 2.** L+S decomposition results at one timepoint of a representative subject's CBF image series. For the simplicity of illustration, only one image slice was displayed. The top row is the sparse component, and the bottom row is the low-rank component. α value used in L+S decomposition was shown beneath each column of the images.

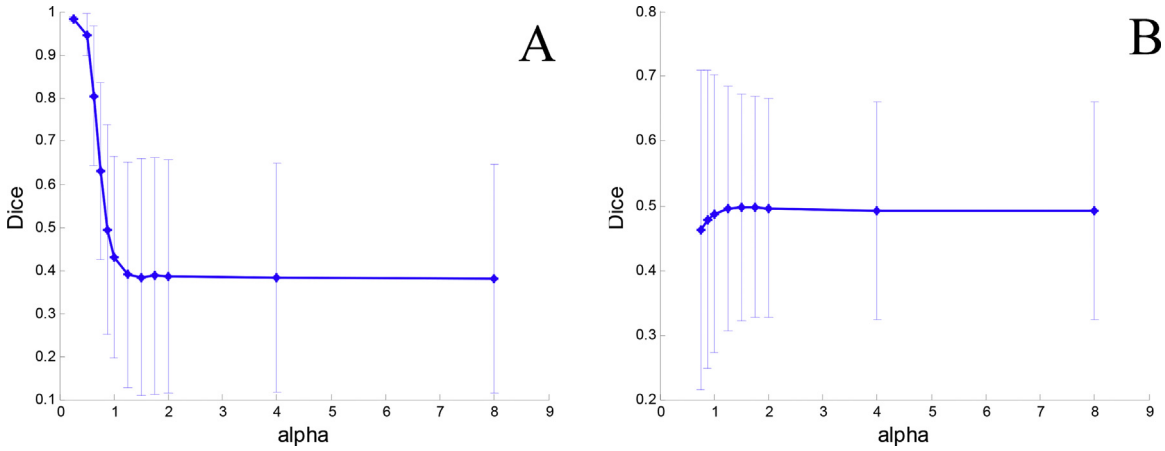


**Fig. 3.** The Dice curves calculated at different alpha values. (A) Dice ratio was calculated from the right motor cortex FC clusters identified from the L+S denoised control images and label images of the resting ASL data. (B) Dice ratio was obtained from sensorimotor function activation clusters detected from the L+S denoised control and label images of the sensorimotor ASL fMRI data. Errorbars indicate the standard deviation.

time series of each voxel in the rest of the brain. The correlation coefficients of all voxels formed the FC map. Because the p values of the individual FC maps were extremely small across the brain, in order to better localize the FC patterns in target regions as reported in the literature, the FC maps w thresholded with an arbitrarily low p value of $1 \times 10^{-5}$ and cluster-size bigger than 100 to identify regions with significant FC to the seed. The overlap ratio between the FC maps of the control image series and the label image series was measured with the Dice index defined by

$$\text{Dice} = \frac{|A \cap B|}{|A \cup B|},$$

where A and B represent the significant FC clusters identified from control and label images, respectively.

In order to identify a value of alpha which will also works for brain activation studies, we performed the same parameter selection process using the sensorimotor ASL fMRI data to be described below. Similar to the resting ASL data, the ASL fMRI data were acquired with a T2*-weighted sequence too. So the control and label image series contained BOLD signal, which can be subsequently used to detect the task activation separately. By applying L+S denoising with different alpha to the control and label image series separately, the Dice index was then defined by the overlap ratio of the task-activation patterns detected from the denoised control image series and label image series. Task detection was based on the general linear model with the task design function convolved with the hemodynamic response function (HRF) as the regressor (more details can be found below).

### 2.6. Temporal signal-to-noise-ratio (TSNR) performance

TSNR was calculated from the ASL CBF images by:

$$\text{TSNR} = \text{meanofthetimeseries/standarddeviationofthetimeseries}.$$

TSNR was averaged across the whole brain as an aggregate performance index to compare the proposed LS-ASLd method with CompCor, using the rest twenty subjects in the resting state ASL data.

### 2.7. FC analyses

Although FC is still widely assessed with BOLD fMRI, ASL MRI directly quantifies CBF and thus provides a more direct and quantitative way to assess regional brain activity and inter-regional FC.

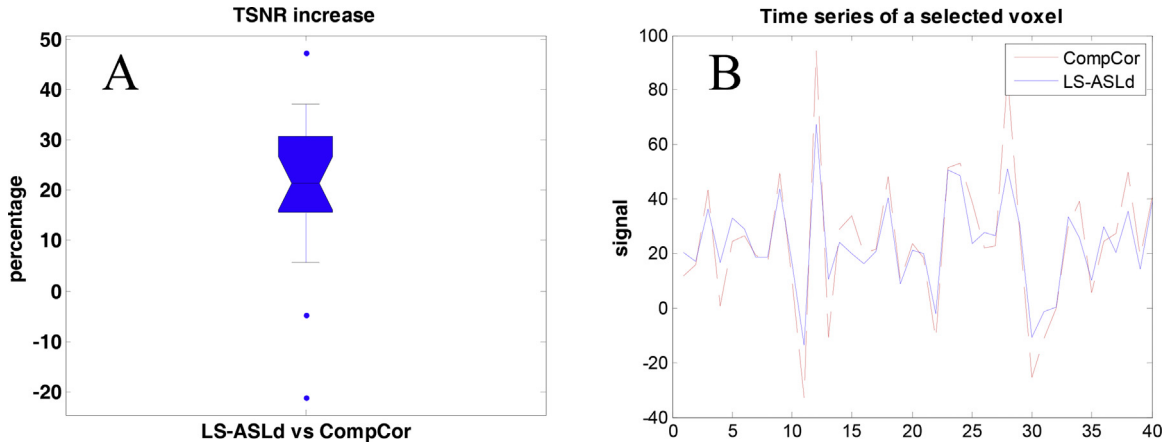


**Fig. 4.** (A) The TSNR increase of LS-ASLd (alpha = 2) compared to CompCor, in which the central mark is the median and edges are the 25th and 75th percentiles. (B) The time series of a selected voxel denoised with CompCor and LS-ASLd (alpha = 2) respectively.

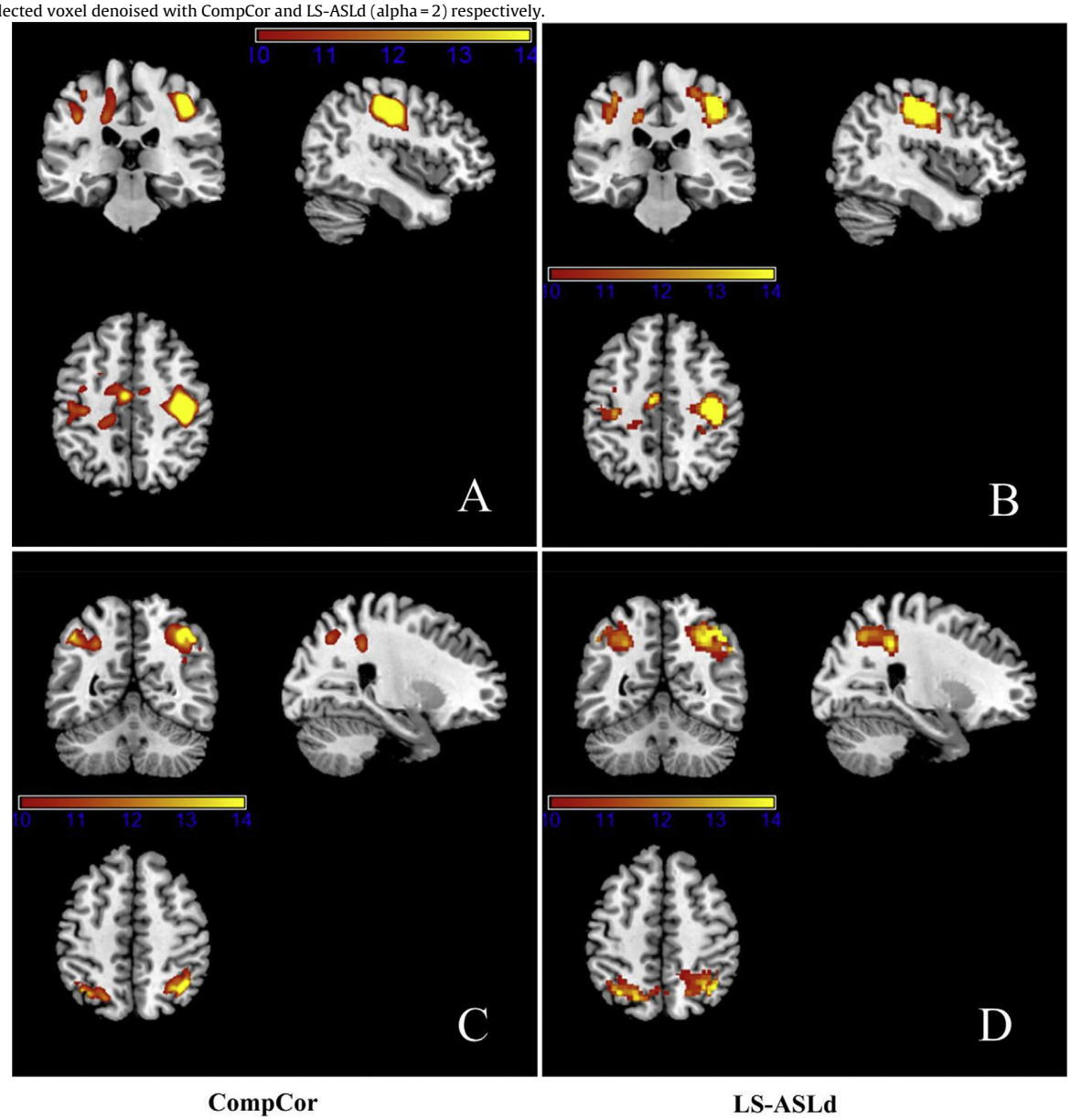


**Fig. 5.** FC patterns identified from CBF images denoised by two different methods. (A) Right motor cortex FC patterns (using the right motor cortex seed) identified from CompCor denoised CBF images. (B) Right motor cortex FC patterns identified from LS-ASLd denoised CBF images. (C) Right parietal cortex FC patterns identified from CompCor denoised CBF images. (D) Right parietal cortex FC patterns identified from LS-ASLd denoised CBF images. Colorbar indicates the display window for the t-values. The positions of the axial, coronal, and sagittal slices are z = 119, y = 99, and x = 133 in the MNI space, in A and B subfigures, and z = 123, y = 71, x = 115 in the MNI space, in C and D subfigures.

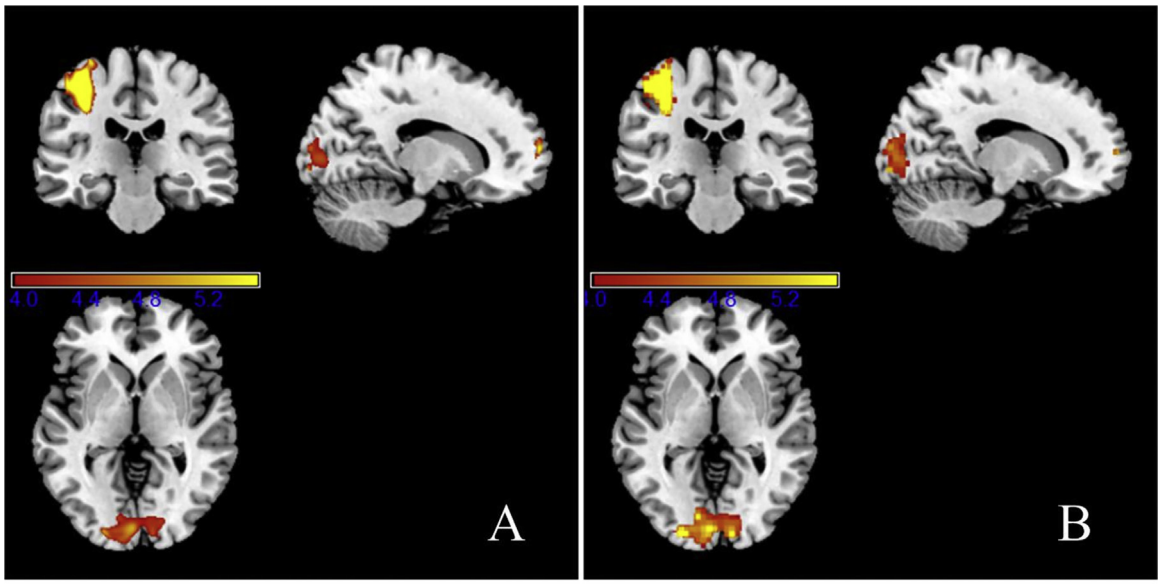


**Fig. 6.** Sensorimotor task activation patterns detected at the group level using ASL CBF images denoised by: (A) CompCor, (B) LS-ASLd. Colorbar indicates the display window for the t-values. The positions of the axial, coronal, and sagittal slices are z = 72, y = 102, and x = 106 in the MNI space, respectively.

However, such kind of temporal analyses based on ASL CBF image series are still hampered by the low sensitivity caused by the low SNR of ASL data. Suppressing temporal noise becomes a critical preprocessing step for those analyses. To verify whether FC analysis can benefit from LS-ASLd, two sets of seed-based FC analyses were performed using the preprocessed CBF images (with CompCor or with LS-ASLd) spatially normalized into the MNI standard brain space. We chose two widely used seeds: the right primary motor cortex and the right parietal cortex. Mean CBF time course was extracted from each seed region for each subject's CBF image series. FC analysis was performed using the same procedure as mentioned above using the mean seed region time series as the regressor. One sample *t*-test was then performed to assess the group level significance of FC at each voxel using the individual FC maps. The same analysis was repeated for each seed and differently processed (with CompCor or with LS-ASLd) CBF data. The statistical results was thresholded with a significance level of $p < 0.0005$ (corrected with the family-wise error method as implemented in SPM12).

### 2.8. Sensorimotor task activation detection

The following analyses were performed using SPM12 through the batch scripts included in ASLtbx. Functional ASL CBF images denoised by CompCor or LS-ASLd were used for identifying brain activations in response to the sensorimotor task performance. At the individual subject level, a general linear model was used to fit the CBF time series at each voxel to the boxcar fMRI task design function convolved with the canonical hemodynamic response function (HRF). A statistical contrast between the sensorimotor task condition and rest condition (equal to a two-sample *t*-test) was then performed to extract the task vs rest brain activity difference. The corresponding contrast maps were spatially registered into the MNI space and then compared at each voxel across all subjects using one-sample *t*-test. The resultant group level statistical results were thresholded with a $p < 0.001$ (uncorrected) and a cluster size>100 (corrected for multiple comparison with alpha <0.05 using Monte Carlo simulation based correction as implemented in AlphaSim (https://afni.nimh.nih.gov/pub/dist/doc/program_help/AlphaSim.html)).

## 3. Experimental results

### 3.1. Parameter selection

Fig. 3 shows the Dice performance curves evaluated at different $\alpha$ values. Fig. 3A is the results obtained from the FC analyses based on the control and label images of the resting ASL data. The right motor cortex was used as the seed. Dice index of FC was close to 1 when $\alpha$ was <1 because more and more signal components were pushed into the sparse element and the resultant L + S denoised images became more and more spatially coherent, resulting in greatly increased FC across the brain. Dice decreased significantly when $\alpha$ increased until 1.25 ($p < 0.05$ for the paired-wise *t*-test between Dice values of $\alpha < 1.25$ and $\alpha = 1.25$). It stayed almost the same value after $\alpha > 2$. Fig. 3B is the results from the sensorimotor fMRI data. Different from the FC Dice curve, the sensorimotor Dice curve first increases then decreases when $\alpha$ increases, indicating two extreme phenomena of the L + S denoising. In the one end when $\alpha$ is too small, too much signal will be treated as sparse noise, resulting in over-denoising; in the other end when $\alpha$ is too big, too little noise will be picked up in the sparse component, resulting in under-denoising. Consistent with Fig. 3A, B shows an optimal range of $\alpha$ between 1.25 and 2. Below we presented results mainly based on $\alpha = 2$.

### 3.2. TSNR performance of LS-ASLd for perfusion ASL images

Fig. 4A shows the boxplot of TSNR increase of LS-ASLd ($\alpha = 2$) compared to CompCor (Behzadi et al., 2007). The percentage of TSNR increase was computed by $100\% \times (\mathrm{TSNR}_{LS-ASLd} - \mathrm{TSNR}_{CompCor})/\mathrm{TSNR}_{CompCor}$ for each subject. LS-ASLd demonstrated 20% TSNR increase compared to CompCor. Fig. 4B shows the time series of a selected voxel from a representative subject denoised with CompCor and LS-ASLd respectively. It illustrates that the spike-like temporal signal component was removed by LS-ASLd.

**Table 1**
Peak location and cluster size of the suprathreshold functional connectivity detected at the group level using ASL CBF images denoised by CompCor or LS-ASLd. Significance level was defined by $p < 0.0005$ (corrected), cluster size > 100 (alpha < 0.05 corrected for multiple comparison using AlphaSim). Note that RMC is the abbreviation of right motor cortex; RPC is the abbreviation of right parietal cortex.

| | CompCor | | | LS-ASLd | | |
|---|---|---|---|---|---|---|
| | (x,y,z) | t | Cluster size | (x,y,z) | t | Cluster size |
| RMC | (42,−22,46) | 60.24 | 1567 | (42,−20,44) | 79.29 | 1565 |
| RPC | (44,−56,44) | 24.27 | 1498 | (40,−60,48) | **26.86** | **1856** |

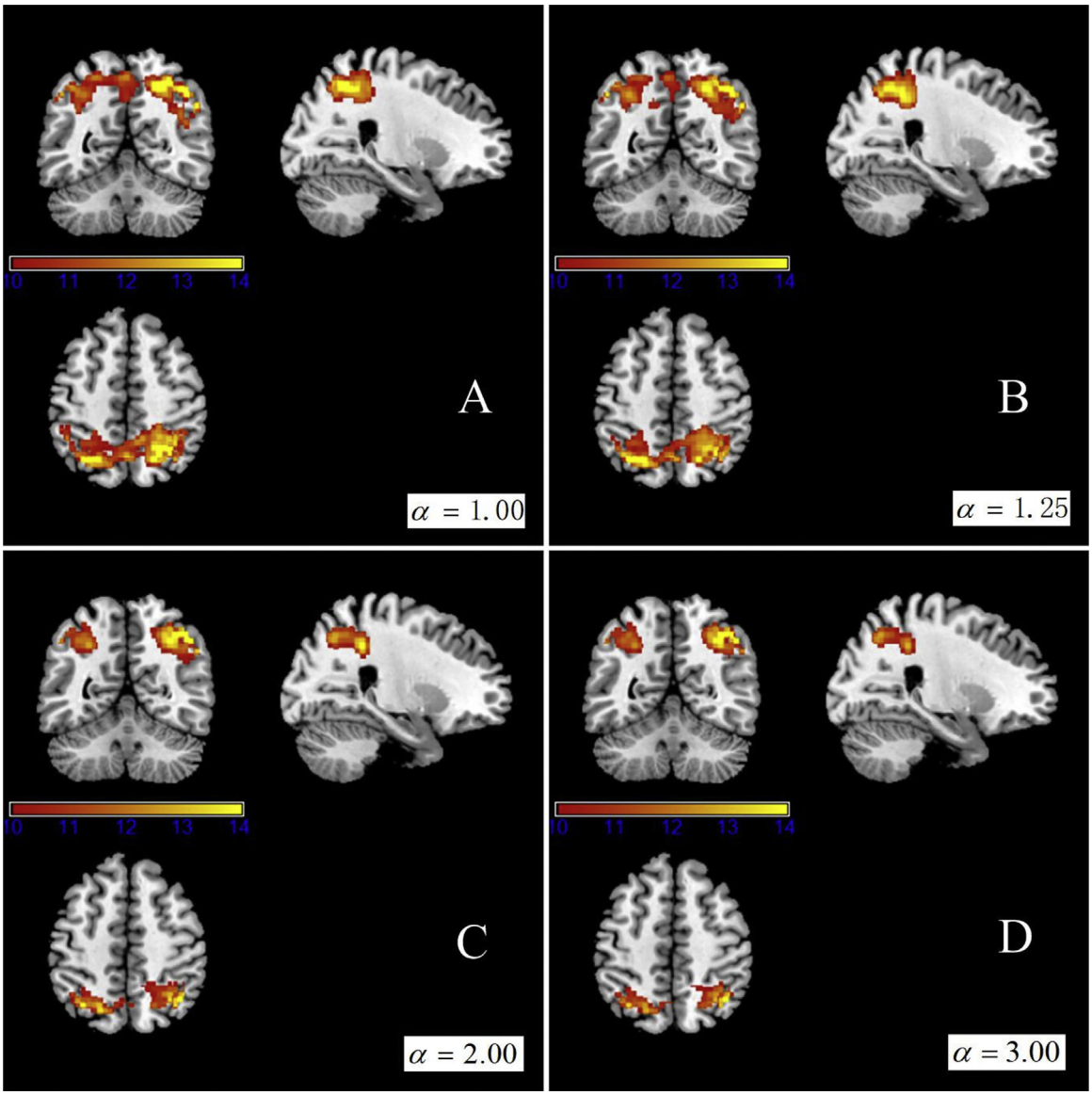


**Fig. 7.** Right parietal cortex FC patterns identified from LS-ASLd denoised CBF images with different parameters: (A) α = 1, (B) α = 1.25, (C) α = 2, (D) α = 3. Colorbar indicates the display window for the t-values. The positions of the axial, coronal, and sagittal slices are z = 123, y = 71, and x = 115 in the MNI space, respectively.

### 3.3. Results of ASL CBF-based FC analysis

Fig. 5 shows the results of ASL CBF-based FC analysis using the right motor cortex seed (Fig. 5A and B) and the right parietal cortex seed (Fig. 5C and D), respectively. Fig. 5A and C shows the FC patterns obtained by the CompCor denoised CBF images, and Fig. 5B and D shows the FC pattern obtained by the LS-ASLd denoised CBF images. Both denoising methods yielded similar typical FC patterns. Motor cortex FC was demonstrated in contralateral motor cortex, and supplementary motor area (SMA). Lateral parietal cortex FC was shown in contralateral brain area as well as precuneus. Table 1 lists the peak t-value and the extent of the suprathreshold clusters of FC analysis using data denoised by CompCor and LS-ASLd, respectively. For the right motor cortex seed, LS-ASLd showed higher peak t value and similar FC cluster size, while for the right parietal cortex seed, LS-ASLd showed higher peak t value and larger cluster size of FC analysis in typical brain regions that are known to have FC to the seed.

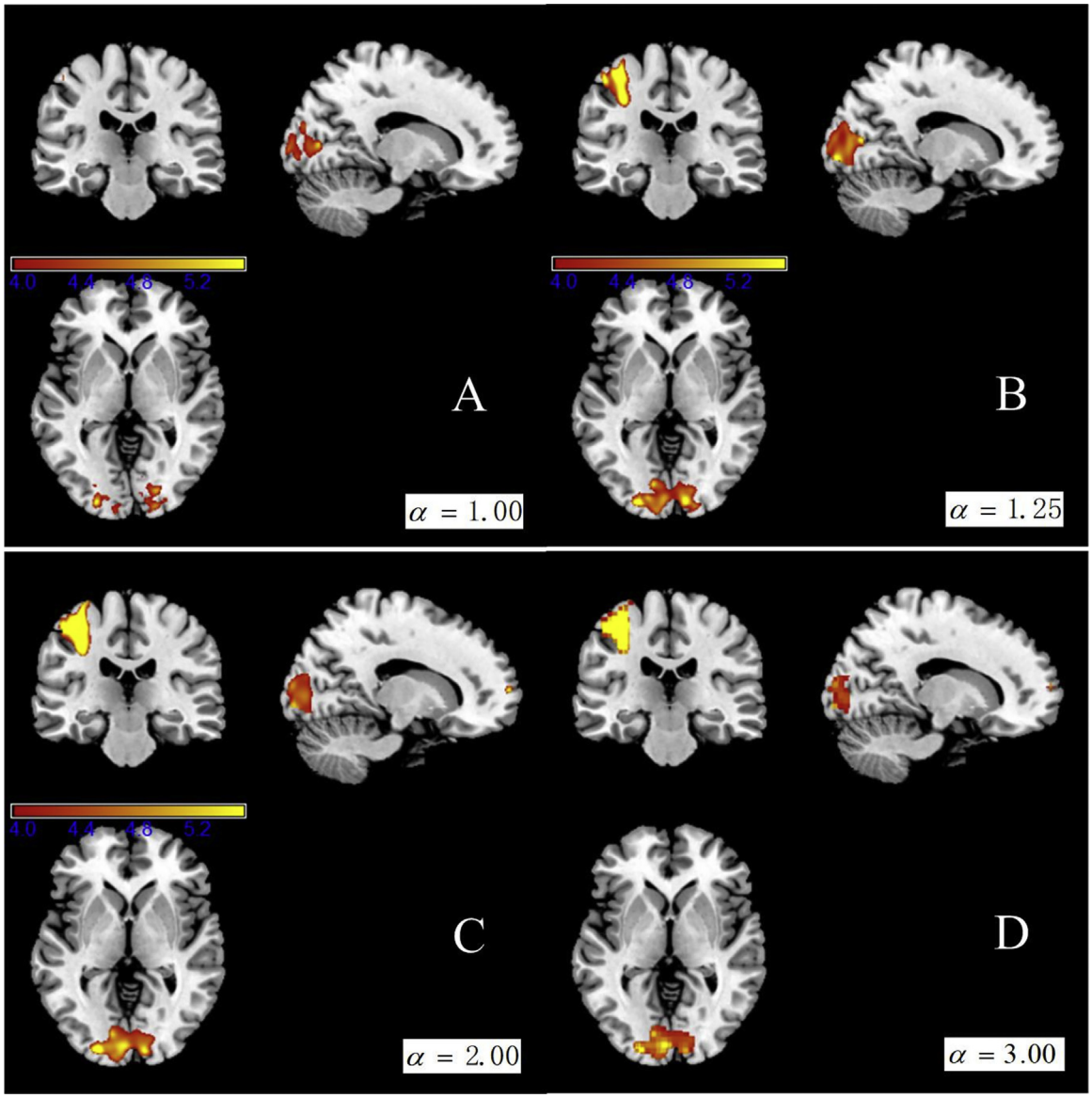


**Fig. 8.** Sensorimotor task activation patterns detected at the group level using ASL CBF images denoised by LS-ASLd with different parameters. Colorbar indicates the display window for the t-values: (A) $\alpha = 1$, (B) $\alpha = 1.25$, (C) $\alpha = 2$, (D) $\alpha = 3$. The positions of the axial, coronal, and sagittal slices are z = 72, y = 102, and x = 106 in the MNI space, respectively.

### *3.4. Results of the sensorimotor task ASL data*

Fig. 6 shows the sensorimotor task activation patterns detected at the group level using ASL CBF images denoised by CompCor (Fig. 6A) and by LS-ASLd (Fig. 6B). Table 2 lists the peak t-values and cluster extension of suprathreshold sensorimotor activation clusters. Two major sensorimotor task activation clusters were detected from the task ASL fMRI data (Fig. 6 and Table 2). LS-ASLd produced higher peak t-value and larger suprathreshold clusters in visual cortex (VC) and motor cortex (MC) than CompCor.

## 4. Discussion and conclusions

Brain perfusion is spatio-temporally coherent, suggesting that the otherwise spatio-temporally incoherent CBF data components can be suppressed as noise. In this study, a spatio-temporal denoising algorithm, LS-ASLd was introduced for ASL fMRI. Using the L+S decomposition (or equivalently rPCA), each ASL CBF map was decomposed into a low-rank component and a sparse component. The former captures the spatio-temporally coherent perfusion signal and the latter represents the spatially and temporally incoherent noise to be removed. Compared to a widely used fMRI temporal denoising method, the Compcor, LS-ASLd improved TSNR by 20%, and resulted in a substantial sensitivity increase for two time-series dependent analyses: FC analysis and task fMRI activation detection. Collectively, these results demonstrated LS-ASLd as a powerful temporal denoising algorithm for ASL MRI with increased sensitivity (in FC and task activation) and specificity (shown in the well-characterized sensorimotor task activation) as compared to the current state-of-art.

L + S decomposition is purely data driven, which can outperform a parametric method such as CompCor in a complex noise environment where noise is difficult to model. While it may seem purely empirical to treat the sparse component as noise, that concept carries the same rationale as that in traditional denoising practices where high frequency signal component is usually considered as noise. Rather than merely requiring the noise to be temporally high-frequency (incoherent), noise in LS-ASLd is also constrained to

**Table 2**
Peak location and cluster size of the suprathreshold sensorimotor task activation patterns detected at the group level using ASL CBF images denoised by CompCor, or LS-ASLd. Significance level was defined by $p < 0.001$ (uncorrected), cluster size > 100 (alpha < 0.05 corrected for multiple comparison using AlphaSim). Note that VC is the abbreviation of visual cortex; MC is the abbreviation of motor cortex.

| | CompCor | | | LS-ASLd | | |
|---|---|---|---|---|---|---|
| | (x,y,z) | t | Cluster size | (x,y,z) | t | Cluster size |
| VC | (−24,−88,4) | 7.6 | 884 | (−24,−90,4) | **9.9** | **1854** |
| MC | (−38,−24,56) | 12.3 | 615 | (−36,−24,56) | **12.4** | **695** |

be spatially sparse, which inherently takes the spatial correlations among neighboring voxels into account and represents an advantage against any univariate method such as CompCor. Removing such temporally and spatially incoherent content of signal resulted in increased TSNR due to the suppression of signal variance. Both increased TSNR and increased spatial coherence induced increased inter-regional correlation, i.e., the FC. For task fMRI, our design is with a low-frequency, so the increased spatial and temporal coherence of the CBF time series would result in increased task activation sensitivity. It is worth to note that, though LS-ASLd differs from CompCor from several aspects, it does not exclude a combination with CompCor or other available temporal ASL denoising methods (Behzadi et al., 2007; Power et al., 2012; Restom et al., 2006; Wang, 2012; Wu et al., 2009).

In LS-ASLd, the regularization parameter $\lambda$ controls the balance of the low-rankness and sparsity of the LS data decomposition and subsequently affects the performance of LS-ASLd. One contribution of this paper was to design a strategy to determine an "optimal" value for $\lambda$. By splitting the raw ASL images into two image series, the control images and the label images, we applied the L + S-based denoising approach to the two series and subsequently ran both FC and GLM analysis. The overlap ratio of the suprathreshold clusters generated from both series was used to find an optimal $\lambda$. The rationale for this empirical approach was because the control and label images still contain BOLD signal and BOLD and ASL CBF are known to yield spatially similar FC patterns or task activation patterns (for the same task) (Chen et al., 2015; Chuang et al., 2008b). While a range of optimal value can be determined from the two Dice curves (one from FC analysis and the other from the sensorimotor fMRI study), we chose $\alpha = 2$ to present our main comparison results. This is not just because it performed well for both FC and GLM, but can also avoid a potential removal of signal of interest. As shown in additional results with different $\alpha$ (Fig. 7 for CBF-based FC, Fig. 8 for CBF-based sensorimotor activation analysis),$\alpha = 2$was a good comprise for both FC and GLM to achieve better performance than CompCor though $\alpha = 1.25$ produced even better results than $\alpha = 2$ for FC analysis. While $\alpha = 2$ was identified from the pseudo-BOLD images, it should be directly applicable to traditional BOLD fMRI though additional validations will be needed.

In summary, we proposed a new temporal ASL CBF image denoising method, LS-ASLd and showed its benefit for the CBF time series-based FC analysis and task activation detection.

## Acknowledgement

The work presented in this paper was supported by National Natural Science Foundation of China, under grant numbers: 61671198 and 61602307; Natural Science Foundation of Zhejiang Province, under grant number: LZ15H180001; the Youth 1000 Talent Program of China; Hangzhou Qianjiang Endowed Professor Program.

## References

Aguirre, G.K., Detre, J.A., Zarahn, E., Alsop, D.C., 2002. Experimental Design and the Relative Sensitivity of BOLD and perfusion fMRI. Neuroimage 15, 488–500.

Alsop, D.C., Detre, J.A., Golay, X., Günther, M., Hendrikse, J., Hernandez-Garcia, L., Lu, H., MacIntosh, B.J., Parkes, L.M., Smits, M., 2015. Recommended implementation of arterial spin-labeled perfusion MRI for clinical applications: a consensus of the ISMRM perfusion study group and the European consortium for ASL in dementia. Magn. Reson. Med. 73, 102–116.

Behzadi, Y., Restom, K., Liau, J., Liu, T.T., 2007. A component based noise correction method (CompCor) for BOLD and perfusion based fMRI. Neuroimage 37, 90–101.

Bibic, A., Knutsson, L., Ståhlberg, F., Wirestam, R., 2010. Denoising of arterial spin labeling data: wavelet-domain filtering compared with Gaussian smoothing. Magn. Reson. Mater. Phys. Biol. Med. 23, 125–137.

Biswal, B.B., Ulmer, J.L., 1999. Blind source separation of multiple signal sources of fMRI data sets using independent component analysis. J. Comput. Assist. Tomogr. 23, 265–271.

Candès, E.J., Li, X., Ma, Y., Wright, J., 2011. Robust principal component analysis? J. ACM (JACM) 58, 11.

Chang, Y.V., Vidorreta, M., Wang, Z., Detre, J.A., 2017. 3D-accelerated, stack-of-spirals acquisitions and reconstruction of arterial spin labeling MRI. Magn. Reson. Med. 78, 1405–1419.

Chen, J.J., Jann, K., Wang, D.J., 2015. Characterizing resting-state brain function using arterial spin labeling. Brain Connect 5, 527–542.

Chiew, M., Smith, S.M., Koopmans, P.J., Graedel, N.N., Blumensath, T., Miller, K.L., 2015. k-t FASTER: Acceleration of functional MRI data acquisition using low rank constraints. Magn. Reson. Med. 74, 353–364.

Chuang, K.-H., Van Gelderen, P., Merkle, H., Bodurka, J., Ikonomidou, V.N., Koretsky, A.P., Duyn, J.H., Talagala, S.L., 2008a. Mapping resting-state functional connectivity using perfusion MRI. Neuroimage 40, 1595–1605.

Chuang, K.H., van Gelderen, P., Merkle, H., Bodurka, J., Ikonomidou, V.N., Koretsky, A.P., Duyn, J.H., Talagala, S.L., 2008b. Mapping resting-state functional connectivity using perfusion MRI. Neuroimage 40, 1595–1605.

Dai, W., Garcia, D., de Bazelaire, C., Alsop, D.C., 2008. Continuous flow-driven inversion for arterial spin labeling using pulsed radio frequency and gradient fields. Magn. Reson. Med. 60, 1488–1497.

Detre, J.A., Leigh, J.S., Williams, D.S., Koretsky, A.P., 1992. Perfusion imaging. Magn. Reson. Med. 23, 37–45.

Fang, R., Huang, J., Luh, W.-M., 2015. A spatio-temporal low-rank total variation approach for denoising arterial spin labeling MRI data. Biomedical Imaging (ISBI). 2015 IEEE 12th International Symposium On. IEEE, 498–502.

Fernández-Seara, M.A., Wang, Z., Wang, J., Rao, H.Y., Guenther, M., Feinberg, D.A., Detre, J.A., 2005. Continuous arterial spin labeling perfusion measurements using single shot 3D GRASE at 3 T. Magn. Reson. Med. 54, 1241–1247.

Kim, S.G., 1995. Quantification of relative cerebral blood flow change by flow-sensitive alternating inversion recovery (FAIR) technique: application to functional mapping. Magn. Reson. Med. 34, 293–301.

Li, Z., Kadivar, A., Pluta, J., Dunlop, J., Wang, Z., 2012. Test-retest stability analysis of resting brain activity revealed by blood oxygen level-dependent functional MRI. J. Magn. Reson. Imaging: JMRI.

Liang, X., Connelly, A., Calamante, F., 2015. Voxel-wise functional connectomics using arterial spin labeling functional magnetic resonance imaging: the role of denoising. Brain Connect. 5, 543–553.

Liao, X.-H., Xia, M.-R., Xu, T., Dai, Z.-J., Cao, X.-Y., Niu, H.-J., Zuo, X.-N., Zang, Y.-F., He, Y., 2013. Functional brain hubs and their test-retest reliability: a multiband resting-state functional MRI study. Neuroimage 83, 969–982.

Lin, Z., Chen, M., Ma, Y., 2010. The Augmented Lagrange Multiplier Method for Exact Recovery of Corrupted Low-rank Matrices. arXiv preprint arXiv:1009.5055.

Liu, T.T., Wong, E.C., 2005. A signal processing model for arterial spin labeling functional MRI. Neuroimage 24, 207–215.

Maleki, N., Dai, W., Alsop, D.C., 2012. Optimization of background suppression for arterial spin labeling perfusion imaging. Magnetic Resonance Materials in Physics. Biol. Med. 25, 127–133.

Maumet, C., Maurel, P., Ferré, J.-C., Barillot, C., 2014. Robust estimation of the cerebral blood flow in arterial spin labelling. Magn. Reson. Imaging 32, 497–504.

Meindl, T., Teipel, S., Elmouden, R., Mueller, S., Koch, W., Dietrich, O., Coates, U., Reiser, M., Glaser, C., 2010. Test-retest reproducibility of the default-mode network in healthy individuals. Hum. Brain Mapp. 31, 237–246.

Otazo, R., Candès, E., Sodickson, D.K., 2015. Low-rank plus sparse matrix decomposition for accelerated dynamic MRI with separation of background and dynamic components. Magn. Reson. Med. 73, 1125–1136.

Power, J.D., Barnes, K.A., Snyder, A.Z., Schlaggar, B.L., Petersen, S.E., 2012. Spurious but systematic correlations in functional connectivity MRI networks arise from subject motion. Neuroimage 59, 2142–2154.

Restom, K., Behzadi, Y., Liu, T.T., 2006. Physiological noise reduction for arterial spin labeling functional MRI. Neuroimage 31, 1104–1115.
Siewert, B., Schlaug, G., Edelman, R.R., Warach, S., 1997. Comparison of EPISTAR and T sub 2*-weighted gadolinium-enhanced perfusion imaging in patients with acute cerebral ischemia. Neurology 48, 673–679.
Singh, V., Tewfik, A.H., Ress, D.B., 2015. Under-sampled functional MRI using low-rank plus sparse matrix decomposition. Acoustics, Speech and Signal Processing (ICASSP), 2015 IEEE International Conference on, 897–901.
Vidorreta, M., Wang, Z., Rodriguez, I., Pastor, M.A., Detre, J.A., Fernandez-Seara, M.A., 2012. Comparison of 2D and 3D single-shot ASL perfusion fMRI sequences. Neuroimage 66C, 662–671.
Vidorreta, M., Wang, Z., Chang, Y.V., Wolk, D.A., Fernandez-Seara, M.A., Detre, J.A., 2017. Whole-brain background-suppressed pCASL MRI with 1D-accelerated 3D RARE stack-Of-Spirals readout. PLoS One 12, e0183762.
Wang, J., Wang, Z., Aguirre, G.K., Detre, J.A., 2005. To smooth or not to smooth?: ROC analysis of perfusion fMRI data. Magn. Reson. Imaging 23, 75–81.
Wang, Z., Childress, A.R., Wang, J., Detre, J.A., 2007. Support vector machine learning-based fMRI data group analysis. Neuroimage 36, 1139–1151.
Wang, Z., Aguirre, G.K., Rao, H., Wang, J., Fernández-Seara, M.A., Childress, A.R., Detre, J.A., 2008. Empirical optimization of ASL data analysis using an ASL data processing toolbox: aSLtbx. Magn. Reson. Imaging 26, 261–269.
Wang, Z., Das, S.R., Xie, S.X., Arnold, S.E., Detre, J.A., Wolk, D.A., Initiative, A.s.D.N., 2013. Arterial spin labeled MRI in prodromal Alzheimer's disease: a multi-site study. NeuroImage: Clin. 2, 630–636.
Wang, Z., 2012. Improving cerebral blood flow quantification for arterial spin labeled perfusion MRI by removing residual motion artifacts and global signal fluctuations. Magn. Reson. Imaging 30, 1409–1415.
Wang, Z., 2014. Support vector machine learning-based cerebral blood flow quantification for arterial spin labeling MRI. Hum. Brain Mapp. 35, 2869–2875.
Wang, Z., 2016. Improving ASL perfusion MRI-based functional connectivity analysis with robust principal component analysis. In: Annual Meeting of ISMRM, Singapore, p. 2873.
Wells, J.A., Thomas, D.L., King, M.D., Connelly, A., Lythgoe, M.F., Calamante, F., 2010. Reduction of errors in ASL cerebral perfusion and arterial transit time maps using image de-noising. Magn. Reson. Med. 64, 715–724.
Wong, E.C., Buxton, R.B., Frank, L.R., 1997. Implementation of quantitative perfusion imaging techniques for functional brain mapping using pulsed arterial spin labeling. NMR Biomed. 10, 237–249.
Wong, E., 1999. Potential and Pitfalls of Arterial Spin Labeling Based Perfusion Imaging Techniques for MRI. Functional MRI, Heidelberg: Springer, pp. 63–69.
Wu, W.-C., Edlow, B.L., Elliot, M.A., Wang, J., Detre, J.A., 2009. Physiological modulations in arterial spin labeling perfusion magnetic resonance imaging. Medical Imaging. IEEE Trans. 28, 703–709.
Ye, F.Q., Frank, J.A., Weinberger, D.R., McLaughlin, A.C., 2000. Noise reduction in 3D perfusion imaging by attenuating the static signal in arterial spin tagging (ASSIST). Magn. Reson. Med. 44, 92–100.